Insights into finding a mismatch through the structure of a mispaired DNA bound by a rhodium intercalator

Valérie C. Pierre, Jens T. Kaiser, and Jacqueline K. Barton*

Division of Chemistry and Chemical Engineering, California Institute of Technology, Pasadena, CA 91125

Contributed by Jacqueline K. Barton, November 15, 2006 (sent for review November 7, 2006)

We report the 1.1-Å resolution crystal structure of a bulky rhodium complex bound to two different DNA sites, mismatched and matched in the oligonucleotide 5′-(dCGG*A*AATTCCCG)$_2$-3′. At the AC mismatch site, the structure reveals ligand insertion from the minor groove with ejection of both mismatched bases and elucidates how destabilized mispairs in DNA may be recognized. This unique binding mode contrasts with major groove intercalation, observed at a matched site, where doubling of the base pair rise accommodates stacking of the intercalator. Mass spectral analysis reveals different photocleavage products associated with the two binding modes in the crystal, with only products characteristic of mismatch binding in solution. This structure, illustrating two clearly distinct binding modes for a molecule with DNA, provides a rationale for the interrogation and detection of mismatches.

DNA recognition | metallointercalator | mismatch detection

Noncomplementary base pairs, or mismatches, within DNA occur during its synthesis via nucleotide misincorporation, inclusion of chemically damaged nucleotides, or inclusion of an undamaged nucleotide opposite a damaged one within the template strand. If left uncorrected, these mismatches lead to mutations upon DNA replication. DNA polymerases generate mismatches at the rate of 10^{-4} to 10^{-5} per base pair at the nucleotide insertion step (1). These mistakes typically are reduced to 10^{-7} per base pair per replication by exonucleases associated with the DNA polymerase and further are reduced 50- to 1,000-fold by the mismatch repair machinery. Deficiencies in mismatch repair increase the rate of mutation and subsequently the risk of developing cancer (2–5).

We have designed rhodium complexes that recognize these sites with high selectivity. Octahedral metal complexes that bind by intercalation previously have been prepared with a range of site selectivities (6). In the case of mismatches, the selectivity is attained (7) with the use of an extended intercalating ligand, such as 5,6-chrysenequinone diimine (chrysi), that is wider than the span of a base pair in normal B form DNA (Fig. 1). Photoexcitation of the rhodium complex cleaves the DNA sugar backbone near the mismatch site. [Rh(bpy)$_2$chrysi]$^{3+}$, for instance, can specifically target a single mismatch in a 2,725-bp plasmid (8). Furthermore, the rhodium complex recognizes and cleaves >80% of mismatch sites in all possible single-base sequence contexts around the mispaired bases (9). These quantitative photocleavage titrations have established that the mismatch-specific binding constants correlate strongly with independent measurements of the thermodynamic destabilization of the mispaired bases. The high specificity of the metal complex in targeting mismatches has led to the application of [Rh(bpy)$_2$chrysi]$^{3+}$ in the discovery of single-nucleotide polymorphisms (10). The complex also selectively inhibits the proliferation of mismatch repair-deficient cells. This unique cell selectivity provides a basis for a strategy for chemotherapeutic design (11, 12).

Furthermore, the binding characteristics of the bulky rhodium complex offer a unique opportunity to explore mechanisms by which mismatch repair proteins as well as base-excision repair proteins may interrogate DNA to find damage. These proteins have the remarkable task of finding the rare occurrences of DNA mispairs and base lesions despite their low copy number, yet the mechanism by which they do so remains to be established (13). In particular, it is debated whether proteins that repair damaged bases search for them by actively flipping out every base consecutively (13, 14), capturing a lesioned base pair that is transiently extrahelical because of its instability (15, 16), or in some manner sensing the damage without extruding the bases (17–20). With unmodified bases that simply are mispaired, extrahelical searches are still more difficult to understand.

Results and Discussion

To improve our understanding of the structural basis for targeting mispaired sites, Δ-[Rh(bpy)$_2$chrysi]$^{3+}$ was cocrystallized with a self-complementary oligonucleotide containing two AC mismatches (5′-$C_1G_2G_3A_4A_5A_6T_7T_8C_9C_{10}C_{11}G_{12}$-3′) for high-resolution x-ray structure determination by the single anomalous diffraction technique (Table 1). The structure, obtained at atomic resolution (1.1 Å), reveals two different binding modes of the metal complex: (*i*) site-specific insertion via the minor groove at the mismatch site with ejection of the two bases and (*ii*) intercalation via the major groove at a matched site (Fig. 1). Although there now are many examples where a single base is flipped out of the DNA duplex, the structure reported here represents an example of insertion of a molecule in DNA with ejection of a base pair.

Minor Groove Insertion at a Mismatched Site. At the thermodynamically destabilized site, Δ-[Rh(bpy)$_2$chrysi]$^{3+}$ inserts in the DNA via the minor groove and ejects both mismatched bases from the double helix (Fig. 2). The mismatched cytosine is extruded into the major groove, where it is positioned in proximity and perpendicular to the π-stacked bases of the helix. In contrast, the ejected mismatched adenosine remains in the minor groove, likely as a result of crystal packing. Indeed, the mismatched adenosine π-stacks both with a bpy ancillary ligand of a rhodium complex inserted in the mismatch site of a crystallographically related DNA and with the adenosine ejected from that same helix. The ejection of the mismatched bases certainly supports

Author contributions: V.C.P. and J.K.B. designed research; V.C.P. and J.T.K. performed research; and V.C.P. and J.K.B. wrote the paper.

The authors declare no conflict of interest.

Abbreviations: chrysi, 5,6-chrysenequinone diimine; phi, 9,10-phenanthrenequinone diimine; (R,R)-Me$_2$trien, 2*R*,9*R*-diamino-4,7-diazadecane.

Data deposition: The coordinates described in this paper have been deposited in the Nucleic Acid Database, Department of Chemistry, Rutgers, The State University of New Jersey, Piscataway, NJ 08854, http://ndbserver.rutgers.edu (NDB structure ID code DD0088; PDB ID 201I).

*To whom correspondence should be addressed. E-mail: jkbarton@caltech.edu.

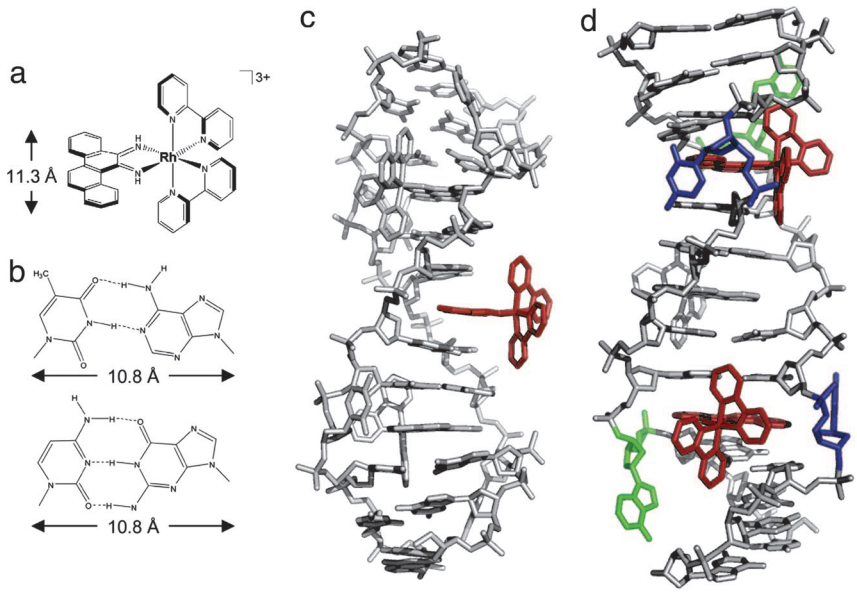

Fig. 1. Overall structure of the rhodium complex bound to the oligonucleotide 5′-CGGAAATTCCCG-3′. (*a*) Chemical structure of Δ- [Rh(bpy)$_2$chrysi]$^{3+}$. (*b*) Watson–Crick base pairs G·C and A·T. (*c*) Intercalation of Δ-[Rh(bpy)$_2$chrysi]$^{3+}$ (red) in the central matched site of the oligonucleotide (gray) via the major groove. (*d*) Insertion of Δ-[Rh(bpy)$_2$chrysi]$^{3+}$ (red) via the minor groove and replacement of the AC mismatch bases. The ejected adenosine (green) remains in the minor groove, whereas the ejected cytosine (blue) is in the major groove.

the correlation between rhodium binding affinity and thermodynamic destabilization of a given mismatch. The rhodium complex inserts deeply within the minor groove, where it

Table 1. Data collection and refinement statistics

Data collection			
	Space group	$P4_32_12$	$P4_32_12$
	Cell dimensions		
	a, *b*, *c*, Å	38.72	38.68
		38.72	38.68
		57.53	57.49
	α, β, γ, °	90	90
		90	90
		90	90
	Wavelength	1.54180	1.03317
	Resolution, Å	25.0–1.6	24–1.14
	R_{merge}*	5.1 (54.0)	6.9 (64.4)
	$I/\sigma I$*	15.7 (2.9)	14.5 (2.4)
	Completeness, %*	100 (100)	100 (99.1)
	Redundancy	3.3†	9.2
Refinement			
	Resolution, Å		1.14
	No. of reflections		16,252
	R_{work}/R_{free}‡		15.1/20.4
	No. of atoms		
	DNA		242
	Intercalators		135
	Water		75
	B factors		
	DNA		22.2
	Intercalator		15.5
	Water		38.3
	rms deviations		
	Bond lengths, Å		0.020
	Bond angles, °		1.2

*Highest-resolution shell is shown in parentheses.
†Redundancy for the CuKα dataset is the anomalous redundancy.
‡Free *R* calculated against 5% of the reflections randomly removed.

π-stacks fully with the flanking AT base pair and with the pyrimidine of the flanking CG base pair; the guanine π-stacks only partially with the chrysi ligand. The chrysi ligand is inserted so deeply in the DNA that it protrudes through the DNA such that it is partially accessible by solvent from the major groove. At this site, the rhodium atom is only 4.7 Å from the helix axis, as compared with the 10-Å radius of B-DNA.

Insertion of the metal complex from the minor groove results only in small conformational changes in the oligonucleotide and is accommodated mainly through opening of the phosphate backbone. Significantly, all sugars maintain C2′-endo puckering, and all bases, including the ejected ones, maintain an *anti* configuration (Tables 2 and 3). The flanking base pairs neither stretch nor shear. Other distortions we observed included buckling and staggering of the external flanking base pairs, which also were observed with the 9,10-phenanthrenequinone diimine (phi) major groove intercalators (21).

Our previous studies on metallointercalators have shown that matching the chirality of the metal complex with that of DNA significantly enhances the binding affinity (22–24). As a result, only the Δ enantiomer of [Rh(bpy)$_2$chrysi]$^{3+}$ cleaves mismatched DNA; no reaction with DNA is observed after photolysis of the Λ enantiomer (7). This enantioselectivity also has been correlated with the higher cytotoxicity of Δ-[Rh(bpy)$_2$chrysi]$^{3+}$ observed in mismatch repair-deficient cell lines as compared with the Λ enantiomer (12). Interestingly, for major groove metallointercalators bound to well matched B-DNA, enantiospecificity is achieved only with complexes containing more bulky ancillary ligands such as for [Rh(5,5′-diphenyl-2,2′-bipyridyl)$_2$phi]$^{3+}$ (24), yet here it is observed with the smaller bpy ligand. The deep insertion of the rhodium complex within the minor groove without an increase in base pair rise provides a structural basis for this enantiospecificity. For insertion from the minor groove into a mismatched site, replacing the Δ enantiomer with the Λ isomer in such a way that the chrysi ligand still π-stacked with the flanking base pairs resulted in significant steric conflict between the ancillary bipyridine ligand and the sugar-phosphate backbone.

Major Groove Intercalation at a Matched Site. Unexpectedly, in the crystal, Δ-[Rh(bpy)$_2$chrysi]$^{3+}$ also was found to intercalate in the

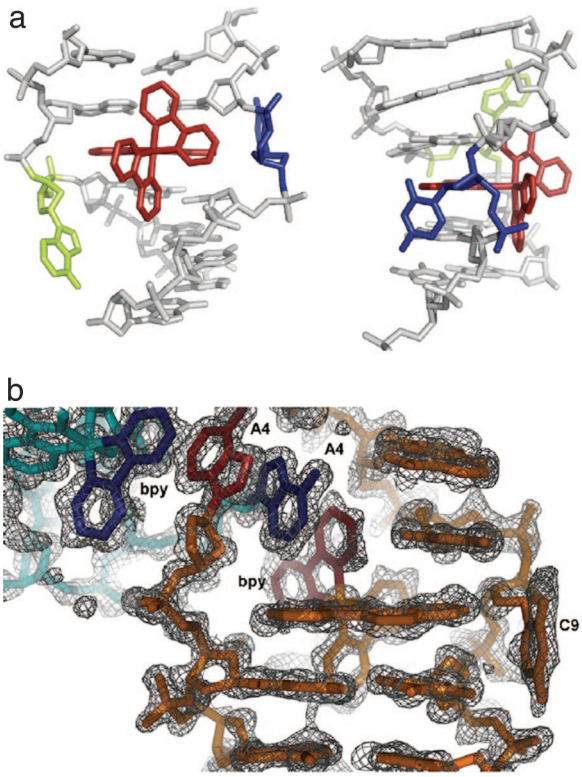

Fig. 2. Insertion of the bulky rhodium complex in the mismatch site. (*a*) Insertion of Δ-[Rh(bpy)$_2$chrysi]$^{3+}$ (red) via the minor groove and replacement of the AC mismatch bases. The ejected adenosine (green) remains in the minor groove, whereas the ejected cytosine (blue) is in the major groove. (*b*) Representative omit $|F_o| - |F_c|$ electron density map for two intertwined and crystallographically related oligonucleotides (orange and cyan). The ejected mismatched adenosine of one strand (red) π-stacks with the 2,2′-bipyridine and ejected adenosine of the related strand (blue).

central 5′-AATT-3′ step of the oligonucleotide from its major groove. In this central site, the rhodium complex intercalates in two different orientations, located on a crystallographic twofold axis, resulting in four rhodium residues of equivalent occupancies. This intercalation has not been detected in solution studies with the rhodium complex and likely is favored by crystal packing. Each ancillary bpy ligand of this central rhodium complex π-stacks with the terminal CG base pair of two crystallographically related oligonucleotides (Fig. 3).

Significantly, this crystal packing provides a direct comparison of two distinct binding modes for the metallointercalator. The complex Δ-[Rh(bpy)$_2$chrysi]$^{3+}$ intercalates in the major groove at the central matched site in a manner similar to that observed for Δ-α-[Rh[(R,R)-Me$_2$trien]phi]$^{3+}$ specifically intercalated in a 5′-TGCA-3′ site (21); the interaction between the intercalating aromatic ligand and the π-orbitals of the bases closely resembles stacking of consecutive base pairs in a DNA duplex. The DNA accommodates the chrysi ligand by opening its phosphate backbone, which results in a doubling of the rise, as well as buckling and staggering of the bases flanking the ligand (Table 3). Although the intercalating chrysi is 0.5 Å wider than the span of a base pair in B form DNA, no shear or stretch was observed in the neighboring base pairs. Furthermore, unlike the phi ligand, which preferentially π-stacks with purines, the chrysi ligand is wide enough to completely overlay with both the purines and pyrimidines of the flanking base pairs. The chrysi ligand does not intercalate as deeply in the major groove as does the phi ligand. Superposition of the structures of the two DNA/metallointercalator complexes indicated that the rhodium atom of Δ-α-[Rh[(R,R)-Me$_2$trien]phi]$^{3+}$ is 1.2 Å closer to the helix axis than that of Δ-[Rh(bpy)$_2$chrysi]$^{3+}$.

Distortion of the Rhodium Complex. Remarkably, the bulky rhodium complex itself distorts in a similar manner both upon intercalation and insertion in the DNA (Fig. 4). Most notably, in the Rh-DNA complex, the chrysi ligand flattens so as to better π-stack with the flanking base pair regardless of the binding mode. In the rhodium complex, the bending of the chrysi ligand is attributed to the steric hindrance between the protonated imine and the hydrogens of C_{25} and C_{37} (25). It is possible that in the intercalated complex, the two imines are deprotonated, thus enabling the chrysi ligand to flatten. The ancillary bpy ligands also are sufficiently flexible to bend within the groove so as to better accommodate the sugar-phosphate backbone. To insert inside the minor groove, the two bpy ligands bend 26° and 12°. Similarly, intercalation in the major groove obliges the two bpys to distort 34° and 19°.

Site-Dependent Photoactivated Cleavage. Because these rhodium complexes are potent photooxidants, this photochemistry has been exploited in marking sites of binding on the DNA duplex (6). Δ-[Rh(bpy)$_2$chrysi]$^{3+}$ specifically cleaves neighboring the mismatch site and, perhaps not surprisingly, with a different product profile than that observed with a major groove intercalator, [Rh(bpy)(phi)$_2$]$^{3+}$ (26, 27). Irradiation of the oligonucleotide-bound metal complex at 365 nm in solution yielded three oxidation products. A first cleavage product, typical of DNA damage, is observed at m/z = 2,802 and corresponds to a 9-mer DNA with a 3′-phosphate terminus (Fig. 5). Two unusual products, which are assigned to a furanone derivative (m/z = 2,898) and a fragment containing a 2,3-dehydronucleotide terminus (m/z = 2,991), characteristically are found after reaction with Δ-[Rh(bpy)$_2$chrysi]$^{3+}$ bound to mismatched DNA but are not observed with major groove

Table 2. DNA conformation of helical parameters relating consecutive base pairs

Parameter*	C/G	G/G	G/A	A/A	A/A	A/T	B-DNA†
Shift, Å	1.07	−0.36	Mismatch	Mismatch	−1.05	0.00	−0.1
Slide, Å	2.31	2.52	—	—	0.69	−0.14	−0.8
Rise, Å	3.24	3.33	—	—	3.14	7.31	3.3
Tilt, °	8.31	−4.82	—	—	−0.19	0.00	−1.3
Roll, °	3.68	7.25	—	—	1.38	−11.86	−3.6
Twist, °	38.00	35.34	—	—	32.20	30.70	36

Data were calculated by using the program 3DNA (40).

*Geometrical relationships between consecutive base pairs: shift, translation into the groove; slide, translation toward the phosphodiester backbone; rise, translation along the helix axis; tilt, rotation about the pseudo-twofold axis relating the DNA strands; roll, rotation about a vector between the C1′ atoms; and twist, rotation about the helix axis.

†Ideal B-form DNA generated by using the program Insight II (BIOSYM/Molecular Simulations, San Diego, CA).

Table 3. DNA conformation of helical parameters relating bases that compose the base pairs

Parameter*	C-G	G-C	G-C	A-C mismatch	A-T	A-T	B-DNA[3]
Shear, Å	0.21	−0.16	−0.30	—	0.02	0.03	0
Stretch, Å	−0.24	−0.21	−0.10	—	−0.08	−0.12	0.1
Stagger, Å	0.49	0.05	0.45	—	0.12	0.28	0.1
Buckle, °	−8.25	4.48	17.65	—	−2.50	10.05	0.1
Propeller, °	−8.45	2.31	−5.06	—	5.84	−8.25	4.1
Opening, °	−2.45	−2.55	−1.02	—	6.04	0.73	−4.1
Sugar pucker	C2′-endo	C2′-endo	C2′-endo	C2′-endo	C2′-endo	C2′-endo	C2′-endo

Data were calculated by using the program 3DNA (40).
*Relationships between the bases that compose the pair, in directions that correspond with those of Table 2.
[†]Ideal B-form DNA generated by using the program Insight II (BIOSYM/Molecular Simulations, San Diego, CA).

intercalators. A second MALDI-TOF mass measurement after 48 h at ambient temperature showed complete conversion of the fragment containing a 2,3-dehydronucleotide terminus ($m/z = 2{,}991$) to the phosphate-modified oligonucleotide. In solution, no DNA cleavage was seen for the chrysi complex with matched DNA. A 2′-deoxyribonolactone, corresponding to the loss of a cytosine base, also appeared at $m/z = 3{,}534$.

Importantly, the photooxidation products directly reflect access of the metal complex to the major or the minor groove of the DNA and can thus be used to assess its binding mode. Strand cleavage via the minor groove is associated with abstraction of H_1', H_4', or H_5' of the deoxyribose ring (28). In the case of Δ-$[Rh(bpy)_2chrysi]^{3+}$, the furanone and the 2,3-dehydronucleotide fragments observed after cleavage at the mismatch site were similar to those of $[Cu(phen)_2]^+$, a minor groove binder that reacts with DNA via H_1' abstraction (29, 30). It is noteworthy that the base propenal and oligonucleotide 3′-phosphoglycolate products characteristic of H_4' abstraction, such as with iron bleomycin, were not observed with the bulky rhodium complex (31, 32). The present structure indicates that insertion of the metal complex via the minor groove positions the bulky ligand in closest proximity to H_1' ($H_1' - C_{chrysi34} = 2.7$ Å). The structure thus corroborates a mechanism for DNA strand cleavage at the mismatch site, where the first step involves H_1' abstraction with subsequent degradation of the deoxyribose ring.

Note that Δ-$[Rh(bpy)_2chrysi]^{3+}$ does not cleave DNA directly at the mismatch site but one base away from the mismatch in the 3′ direction and on the 5′ strand only. In the oligonucleotide crystallized, for instance, cleavage does not occur at the mismatched cytosine but at its flanking pyrimidine (Fig. 5). The present structure provides an explanation for this observation as well. Indeed, ejection of the two mismatched bases positions the deoxyribose protons of the flanking C_{10} significantly closer to the chrysi ring than that of the mismatched C_9.

Accordingly, the present crystal structure, like the structure of Δ-α-$[Rh[(R,R)\text{-}Me_2trien]phi]^{3+}$ (21), also indicates that intercalation via the major groove positions the chrysi ligand close to the H_2' of the sugar ring ($H_2' - C_{chrysi27} = 2.9$ Å). Consistent with other mechanistic studies (27), we propose that for major groove intercalators, the initial oxidative reaction involves abstraction of H_2', followed by hydrogen migration to form the C_3' radical and subsequent degradation of the sugar ring. Notably, irradiation of crystals of the Rh-DNA complex but not in solution also results in strand cleavage, both at the matched and the mismatched positions with expected reaction products (Fig. 5). Analysis of the cleavage products, characteristic of each mechanism, thus may directly assess the binding mode of a metal complex with DNA.

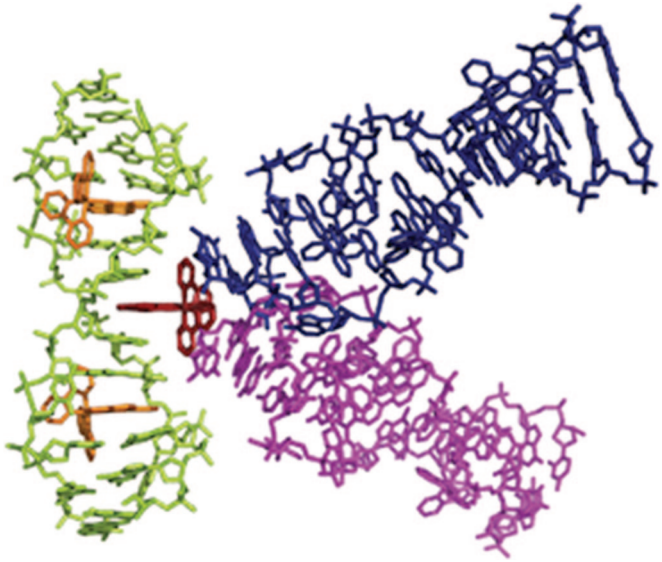

Fig. 3. Crystal packing and π-stacking among three crystallographically related oligonucleotides. Each ancillary bipyridine ligand (red) of the rhodium complex intercalated in the matched site of an oligonucleotide (green) π-stacks with the terminal GC base pair of a related oligonucleotide (blue and magenta).

Recognition of a Thermodynamically Destabilized Site by Ejecting the Mispair. The crystal structure enables us to compare directly the two different binding modes for this metallointercalator: intercalation in matched DNA and insertion in the mismatched site. The comparison furthermore illustrates how the mismatched versus matched site may be distinguished. Intercalation of a complex occurs via the major groove and is typified by a doubling of the rise and no ejection of bases. On the contrary, insertion of a complex occurs via the minor groove and is characterized by ejection of the destabilized mismatch with no change in rise. The differing major and minor groove orientations for these binding modes also lead to distinct photochemical strand cleavage reactions. Furthermore, the large width of the major groove does not sterically hinder the ancillary bipyridine ligands of the complex and can accommodate both the Δ and Λ isomers, whereas the narrow width of the minor groove can only lodge the Δ enantiomer within the right-handed B-DNA helix. These findings are in accordance with the low enantioselectivity observed for the major groove intercalator $[Rh(phen)_2phi]^{3+}$ in contrast to the enantiospecificity observed for $[Rh(bpy)_2chrysi]^{3+}$. Significantly, the bulky chrysi ligand intercalates shallowly in the more open major groove (Rh − helical axis distance = 5.8 Å) but deeply in the more sterically hindered minor groove (Rh − helical axis distance = 4.7 Å), indicating that steric hindrance is not a discriminating factor for minor groove insertion.

The structure thus illustrates a clear strategy for mismatch

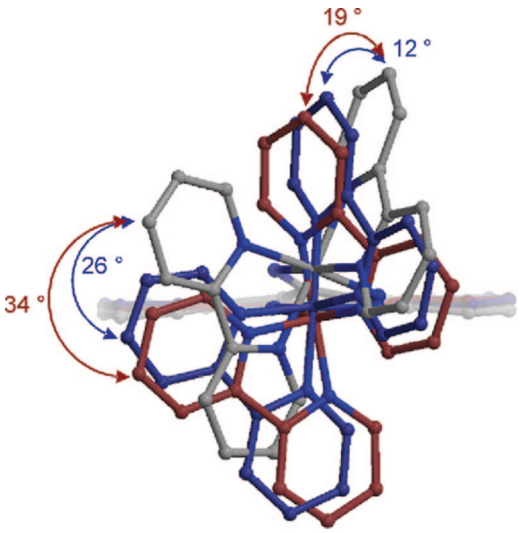

Fig. 4. Distortion of the rhodium complex upon intercalation and insertion in DNA. The crystal structures of Δ-[Rh(bpy)$_2$chrysi]$^{3+}$''free'' (without DNA, gray carbon atoms), inserted via the minor groove (light blue carbon atoms), and intercalated via the major groove (red carbon atoms) were superimposed by using the central ring of the chrysi ligand.

recognition. Although it is conceivable that the mispaired bases can be partially extrahelical transiently in the absence of proteins (33), the presence of a mismatch does not noticeably alter the geometry of DNA, and the bases are intrahelical (34). The rhodium complex recognizes the mismatched site without consecutively interrogating every base extrahelically; rather, it is the local instability of the mismatch that enables Δ-[Rh(bpy)$_2$chrysi]$^{3+}$ to eject the bases. Importantly, the metal complex does not eject the well paired bases but intercalates between them. These different binding modes for matched and mismatched DNA underscore a similar strategy by which repair proteins may examine DNA, where no extrahelical interrogation of each base pair is required.

This 1.1-Å resolution crystal structure therefore reveals with atomic detail the structural basis for the recognition of thermodynamically destabilized mismatched sites in DNA and enables a direct comparison with intercalation at a matched site. As such, the structure illuminates a potential strategy for interrogation of DNA by repair proteins that does not involve sequential extrahelical interrogation of each base to detect lesions. Rather, it is the local instability of the mismatch that favors ejection only of mismatched bases.

Materials and Methods

Synthesis, Purification, and Crystallization. The rhodium complex Δ-[Rh(bpy)$_2$chrysi]$^{3+}$ was synthesized and isolated enantiomerically pure as described (7). Synthetic oligonucleotides were purified by two rounds of reverse-phase HPLC using a C18 column (Varian, Palo Alto, CA). Annealed oligonucleotides were incubated with the rhodium intercalator before crystallization. Subsequent manipulations were performed with minimal exposure of the complex to light. Bright orange crystals were grown from a solution of 1 mM double-stranded oligonucleotide, 3.4 mM enantiomerically pure Δ-[Rh(bpy)$_2$chrysi]$^{3+}$, 20 mM NaCacodylate (pH 7.0), 6 mM spermine·4HCl, 40 mM $SrCl_2$, 10

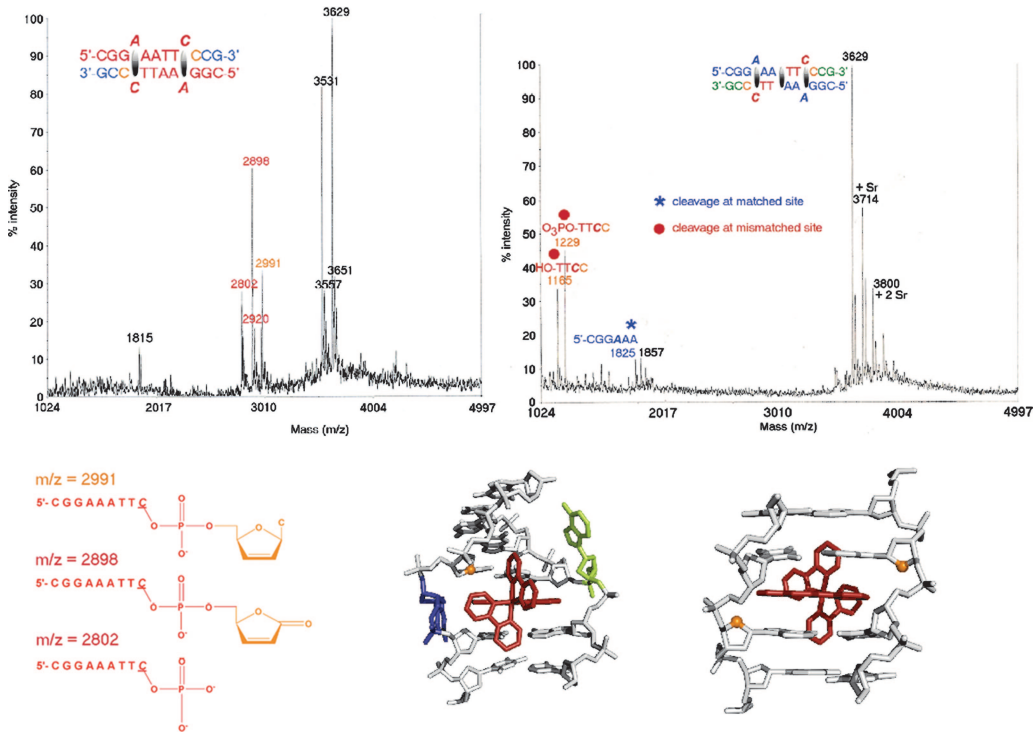

Fig. 5. Photocleavage in solution and in the crystal. MALDI-TOF mass spectra obtained after photocleavage in solution (*Upper Left*) and of the crystal (*Upper Right*). The assignment of the fragmentation has been confirmed by gel electrophoresis. Note that the collection of fragments evident at 2,800–3,000 with photocleavage in solution is not apparent in the crystal. Our assignments for these fragments are provided (*Lower Left*). The data for the crystal are consistent with additional cleavage of these fragments also at the matched site, leading to the appearance of new smaller products at 1,229 and 1,165 corresponding to 5′-TTCC, including the cytosine one base away from the mismatch. The product at 1,825 reflects cleavage only at the matched site yielding 5′-CGGAAA-phosphate. The colors in the duplex sequences above reflect the correspondence with the mass spectral fragments. Also shown below are views of the mismatched site (*Lower Center*) and matched site (*Lower Right*), where the H′ positions closest to the chrysi ligand, H_1' of C_{10} for the mismatched and H_2' of A_6 for the matched, are highlighted in orange. The photocleavage products are consistent with H abstraction from these positions.

mM $MgCl_2$, and 5% 2-methyl-2,4-pentanediol (MPD) equilibrated in sitting drops versus a reservoir of 35% MPD at ambient temperature. Thirteen different sequences were screened before crystals were obtained with 5′-CGGAAATTCCCG-3′. Crystals grew in space group $P4_32_12$ with unit cell dimensions $a = b = 38.7$ Å and $c = 57.6$ Å, and half of a biomolecule per asymmetric strand, with one disordered rhodium on a special position.

Data Collection. The data first were collected from a flash-cooled crystal at 100 K on an R-axis IV image plate by using CuKα radiation produced by a Rigaku (Tokyo, Japan) RU-H3RHB rotating-anode generator with double-focusing mirrors and an Ni filter and then processed with MOSFLM and SCALA from the CCP4 suite of programs (35). Subsequently, data collected on beamline 11–1 at the Stanford Synchrotron Radiation Laboratory (Menlo Park, CA; $\lambda = 1.03$ Å, Quantum 315 CCD detector, 100 K) was merged with the low-resolution data for refinement.

Crystal Structure Determination and Refinement. The crystal was solved by single anomalous dispersion using the anomalous scattering of rhodium ($f'' = 3.6$ electrons for Rh at $\lambda = 1.54$ Å) with the Shelxc/d/e suite of program (36, 37) on the data obtained with CuKα radiation. We located 1.5 heavy atoms per asymmetric unit, with 1 atom on a special position. The structure then was refined by using the program ShelxH (38, 39) against 1.1-Å data to a final $R_1 = 15.2\%$ and $R_{free} = 20.4\%$. The rhodium complex located on the crystallographic twofold axis perpendicular to the helical axis of the DNA intercalates in two different orientations, resulting in four disordered residues of equivalent occupancies. In the later stage of refinement, individual anisotropic B factors were refined, and riding hydrogens were included. Figures were drawn with Pymol (DeLano Scientific, San Carlos, CA).

Photoactivated Cleavage Experiments. Photoactivated cleavage of the DNA by Δ-$[Rh(bpy)_2chrysi]^{3+}$ in solution was analyzed under conditions similar to those used to grow the crystal. The oligonucleotide (200 μM dsDNA) was annealed in 20 mM NaCacodylate (pH 7.0), 40 mM $SrCl_2$, and 10 mM $MgCl_2$. Δ-$[Rh(bpy)_2chrysi]^{3+}$ (680 μM) was added, and the orange solution was irradiated for 1 h at 365 nm. Similarly, for photocleavage of the crystallized DNA, a crystal enclosed in a glass capillary was irradiated for 4 h at 365 nm at ambient temperature and redissolved in water before characterization.

The reaction mixtures were desalted by using the ZipTip procedure. ZipTip C18 columns were equilibrated, and the oligonucleotides were bound, washed, and eluted in 10 μl of acetonitrile/water as described in the procedure for oligonucleotides (Millipore, Billerica, MA). The oligonucleotides then were dried on a speedvac and redissolved in 1 μl of water. The MALDI-TOF mass spectra were measured on a PerSeptive Biosystems Voyager-DE Pro instrument. The samples were prepared by the dry droplet method, using 3-hydroxypicolinic acid as matrix.

We thank M. Day for assistance in structure refinement, D. C. Rees for valuable discussions, and B. M. Zeglis for assistance in the gel electrophoresis experiments. We acknowledge support from the National Institutes of Health (Grant GM33309) and the Gordon and Betty Moore Foundation to the Caltech Molecular Observatory. The rotation camera facility at Stanford Synchrotron Radiation Laboratory is supported by the U.S. Department of Energy and National Institutes of Health.

1. Iyer RR, Pluciennik A, Burdett V, Modrich PL (2006) *Chem Rev* 106:302–323.
2. Kunkel TA, Erie DA (2005) *Annu Rev Biochem* 74:681–710.
3. Strauss BS (1999) *Mutat Res* 437:195–203.
4. Arzimanoglou II, Gilbert F, Barber HRK (1998) *Cancer* 82:1808–1820.
5. Loeb LA, Loeb KR, Anderson JP (2003) *Proc Natl Acad Sci USA* 100:776–781.
6. Erkkila KE, Odom DT, Barton JK (1999) *Chem Rev* 99:2777–2795.
7. Jackson BA, Barton JK (1997) *J Am Chem Soc* 119:12986–12987.
8. Jackson BA, Alekseyev VY, Barton JK (1999) *Biochemistry* 38:4655–4662.
9. Jackson BA, Barton JK (2000) *Biochemistry* 39:6176–6182.
10. Hart JR, Johnson MD, Barton JK (2004) *Proc Natl Acad Sci USA* 101:14040–14044.
11. Junicke H, Hart JR, Glebov O, Kirsch IR, Barton JK (2003) *Proc Natl Acad Sci USA* 100:3737–3742.
12. Hart JR, Glebov O, Ernst R., Kirsch IR, Barton JK (2006) *Proc Natl Acad Sci USA* 103:15359–15363.
13. Verdine GL, Bruner SD (1997) *Chem Biol* 4:329–334.
14. Banerjee A, Yang W, Karplus M, Verdine GL (2005) *Nature* 434:612–618.
15. Duguid EM, Mishina, Y He C (2003) *Chem Biol* 10:827–835.
16. Viadiu H, Aggarwal AK (2000) *Mol Cell* 5:889–895.
17. Boal AK, Yavin E, Lukianova OA, O'Shea VL, David SS, Barton JK (2005) *Biochemistry* 44:8397–8407.
18. Boon EM, Livingston AL, Chmiel NH, David SS, Barton JK (2003) *Proc Natl Acad Sci USA* 100:12543–12547.
19. Junop MS, Obmolova G, Rausch K, Hsieh P, Yang W (2001) *Mol Cell* 7:1–12.
20. Banarjee A, Santos WL, Verdine GL (2006) *Science* 311:1153–1157.
21. Kielkopf CL, Erkkila KE, Hudson BP, Barton JK, Rees DC (2000) *Nat Struct Biol* 7:117–121.
22. Barton JK (1986) *Science* 233:727–734.
23. Johann TW, Barton JK (1996) *Philos Trans R Soc London A* 354:299–324.
24. Sitlani A, Dupureur CM, Barton JK (1993) *J Am Chem Soc* 115:12589–12590.
25. Jackson BA, Henling LM, Barton JK (1999) *Inorg Chem* 38:6218–6224.
26. Brunner J, Barton JK (2006) *J Am Chem Soc* 128:6772–6773.
27. Sitlani A, Long EC, Pyle AM, Barton JK (1992) *J Am Chem Soc* 114:2303–2312.
28. Pogozelski WK, Tullius TD (1998) *Chem Rev* 98:1089–1107.
29. Meijler MM, Zelenko O, Sigman DS (1997) *J Am Chem Soc* 119:1135–1136.
30. Goyne T, Sigman DS (1987) *J Am Chem Soc* 109:2846–2848.
31. Stubbe J, Kozarich JW (1987) *Chem Rev* 87:1107–1136.
32. Kozarich JW, Worth L, Frank BL, Christner DF, Vanderwall DE, Stubbe J (1989) *Science* 245:1396–1399.
33. Priyakumar UD, MacKerell AD, Jr (2006) *Chem Rev* 106:489–505.
34. Hunter WN, Brown T, Kennard O (1987) *Nucleic Acids Res* 15:6589–6606.
35. Collaborative Computational Project, Number 4 (1994) *Acta Crystallogr D* 50:760–763.
36. Schneider TR, Sheldrick GM (2002) *Acta Crystallogr D* 58:1772–1779.
37. Sheldrick GM (2002) *Z Kristallogr* 217:644–650.
38. Sheldrick GM, Schneider T (1997) *Methods Enzymol* 277:319–343.
39. Parkinson G (1996) *Acta Crystallogr D* 52:57–64.
40. Lu X-J, Olson WK (2003) *Nucleic Acids Res* 31:5108–5121.